

THE MAXIMUM EXCESS TEMPERATURE OF FIRE-INDUCED SMOKE FLOW BENEATH AN UNCONFINED CEILING AT HIGH ALTITUDE

by

**Jiahao LIU^a, Zhihui ZHOU^b, Jian WANG^{c*},
Qimiao XIE^a, Jinhui WANG^a, and Richard YUEN^d**

^a College of Ocean Science and Engineering, Shanghai Maritime University, Shanghai, China

^b China Waterborne Transport Research Institute, Beijing, China

^c State Key Laboratory of Fire Science,
University of Science and Technology of China, Hefei, China

^d Department of Architecture and Civil Engineering,
City University of Hong Kong, Hong Kong, China

Original scientific paper

<https://doi.org/10.2298/TSCI170926075L>

Conventional correlations for the maximum temperature under a ceiling were mainly developed based on the experimental results at atmospheric pressure. For high-altitude environment with lower ambient pressure, their feasibility needs to be reexamined. In this paper, a sequence of pool fires with different dimensions and fuel types was performed under a horizontal unconfined ceiling to measure the maximum excess temperature in a high-altitude city, Lhasa (3650 m/64.3 kPa). The results show that the maximum smoke temperatures beneath the ceiling at high altitude are significant higher than the predicted values by Alpert's model. Considering the effects of ambient pressure and entrainment coefficient, a new theoretical model for predicting the maximum excess temperature was proposed based on the ideal plume assumption. The current results together with the data in the literature which conform with Alpert's model successfully converge by employing the proposed correlation.

Key words: *maximum excess temperature, high-altitude environment, pool fire, ceiling jet*

Introduction

In case of fires occurred in compartments or tunnels, hot gases in the fire plume rise directly above the burning fuel and impinge on the ceiling, and then move horizontally under the ceiling to areas remote from the fire source [1]. A series of numerical and experimental investigation concerning the temperature distribution and heat flux beneath the ceiling has been conducted in past decades, which plays an important role in fire safety design of buildings [2-5], tunnels [6-8], cargo compartments [9, 10] and so on.

The maximum temperature under the ceiling usually serves as the trigger for the flame spread along the ceiling, and the ceiling temperature decay profile is particularly critical for the selection of multi-sensor detection methods [11]. To investigate the regularity of these parameters, studies pertaining to the theories of the impingement of a fire plume were initially conducted by Alpert [12, 13] and by Heskestad *et al.* [14]. Based on the experimental results, Alpert established a generalized theory to correlate the gas velocity, gas temperature distribution for

* Corresponding author, e-mail: wangj@ustc.edu.cn

a weak plume under an unconfined ceiling as the flame height was much lower than the height of the ceiling above the fire source [12]. Subsequently, the new correlations of non-dimensional velocity and temperature, applicable to a wider range of ceiling height, were proposed by Heskestad *et al.*, [14]. However, these correlations or theoretical analysis were developed on the basis of the experimental results at atmospheric pressure, and their feasibility under some extreme environments, such as at high altitude cities or cruising aircrafts with lower ambient pressures, has not been validated.

Both the field and chamber tests have indicated that the low pressure environment will significantly affect the combustion behaviors [15, 16]. The experiments conducted at high-altitude have indicated that the low pressure environment will prolong the alarm time of fire detectors and even cause the failure of them [17]. To investigate the low pressure effect on the ceiling temperature profile which affects the activation of fire detectors for aircraft cargo compartment fires, Wang *et al.* [10] performed a sequence of *n*-heptane pool fires in the pressure range of 70~100 kPa. Their findings showed that apart from the ambient pressure, the air entrainment coefficient also played an important role in affecting the ceiling temperature profile. However, Liu *et al.* [18] compared the results of small-scale pool fires obtained by field tests and their corresponding chamber tests (performed in a 12 m³ altitude chamber), and found that small to significant difference in mass loss, axial temperature profile and flame envelop can be observed between them. The enclosure effect caused by the altitude chamber or cargo compartment will inevitably result in different ceiling temperature profile from the tests in an open space.

With the sustained economic prosperity, more modern buildings are being constructed at high-altitude areas, such as Qinghai-Tibet Plateau, while their fire safety design usually imitates the prescribed rules developed from the experiments at atmospheric pressure. Considerable studies concerning the burning behaviors at various pressures have demonstrated that low air pressures has significant effects on the fire properties and smoke flow [10, 15-18]. During a fire, the construction of a ceiling will either be damaged by the induced hot smoke or the hitting of the flames, or a combination of both. The maximum excess temperature right above the fire source is the greatest threat to the integrality of the ceiling. Thus, the aim of this work is to quantitatively acquire the maximum excess temperature under an unconfined horizontal ceiling at high-altitude environment. Based on that, it is expected to establish an empirical model to accurately predict this critical parameter to offer guidance for fire safety design in buildings at high altitude.

Thus, to achieve the goal, a series of pool fires with different pool dimensions and fuel types were performed under a ceiling at high altitude to mimic the weak plume driven ceiling jet. All the experiments were conducted in an EN54 standard combustion room built in Lhasa with the altitude of 3650 m and the pressure of 64.3 kPa. The maximum excess temperature under the ceiling were carefully analyzed and compared with Alpert's empirical model to extend its application at high-altitude environment.

Experimental descriptions

To directly acquire basic data of fires at high altitude, a plateau fire laboratory was formally established in a fire training base, located in Lhasa city, Tibet Autonomous Region, China, in July 2009. Since then, considerable experiments were conducted to investigate the pressure effect on the combustion behaviors. The overall appearance of the laboratory is illustrated in fig. 1(a), where the experimental site, EN54 standard combustion room with dimensions of 7 m wide, 10 m long, and 4 m high, is marked. Two extra pictures showing the interior

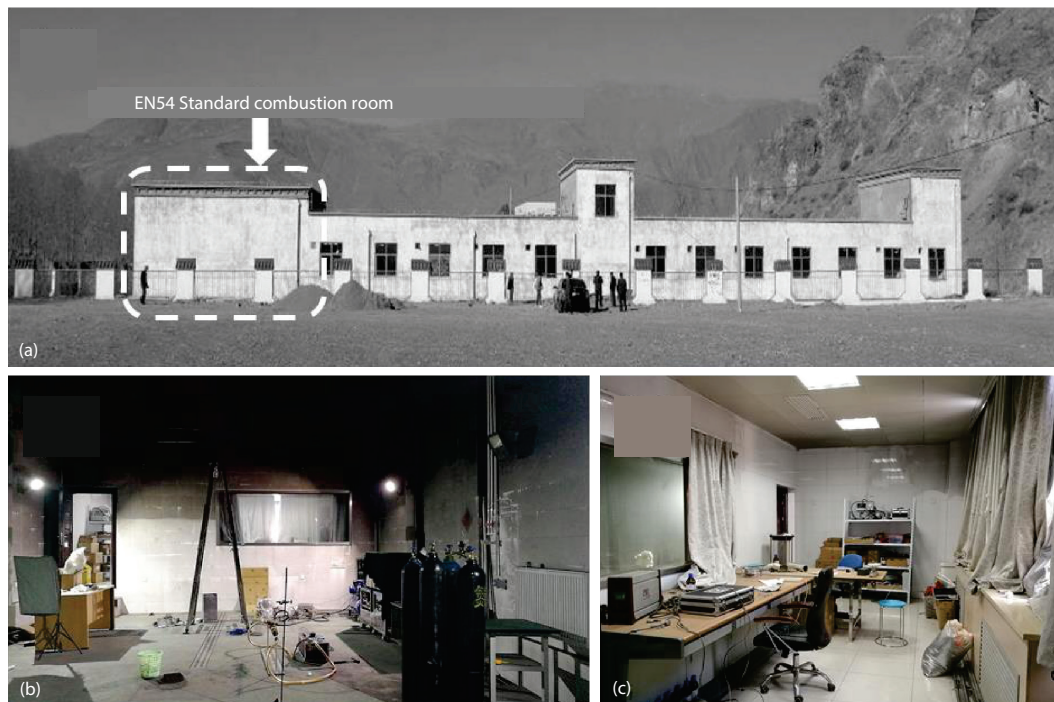


Figure 1. The picture of EN54 standard combustion room in Lhasa; (a) the overall appearance of the plateau fire laboratory, (b) interior lay-out of the room, and (c) observation room

lay-out and observation room of the laboratory are presented in figs. 1(b) and 1(c), respectively. During the test, the windows and doors of the room were closed, but not sealed, to prevent disturbance (especially wind effect) from outside. The gas exchange could occur through the leaks around the room to maintain the pressure equilibrium with the outside ambient, *i. e.* 64.3 kPa.

The experimental set-up is illustrated in fig. 2, where the fig. 2(a) is the photo during the fire test, figs. 2(b) and 2(c) are the photos of electronic scale and thermocouple, respectively, and the schematic diagram of the experiments is given in fig. 2(d). A $1\text{ m} \times 1\text{ m}$ square mica smooth plate with low thermal conductivity of $0.035\text{ Wm}^{-1}\text{K}^{-1}$ and excellent heat resistance performance was supported by four iron stands to serve as the ceiling. The oil pan is placed upon an electronic scale (Mettler-Toledo XP10002S) with the precision of 0.01 g to monitor the mass loss during the tests. A $20\text{ cm} \times 20\text{ cm}$ square insulation board is positioned between them to shield the scale from the elevated temperature. Three sizes of round fuel pans, *i. e.* 10 cm, 14 cm, and 20 cm in diameter, were employed in current study. The height of all pans was 2 cm and the steel thickness was $0.32 \pm 0.01\text{ cm}$. Three types of fuels with different sooting levels, *i. e.* ethanol (weakly-sooting), *n*-heptane (moderately-sooting) and jet-A (heavily-sooting) [4, 19], were used in current study, and the specific property parameters of these fuels were listed in tab. 1. In each test, the fuel pan was fueled to a height of 1.5 cm with $\pm 5\%$ variation, and the weight of fuel for different pool dimensions and fuel types could be estimated by the utilization of the density of the fuels. For all the tests, the fuels were ignited with a butane lighter. Because the jet-A fuel is difficult to be ignited directly, a small amount of ethanol (5 mL, about 3.9 g) was poured on the surface of the fuel as ignition source. The mass of the ignition agent is about 3% initial weight of $D = 10\text{ cm}$ jet-A fuel and thus can be reasonably neglected.

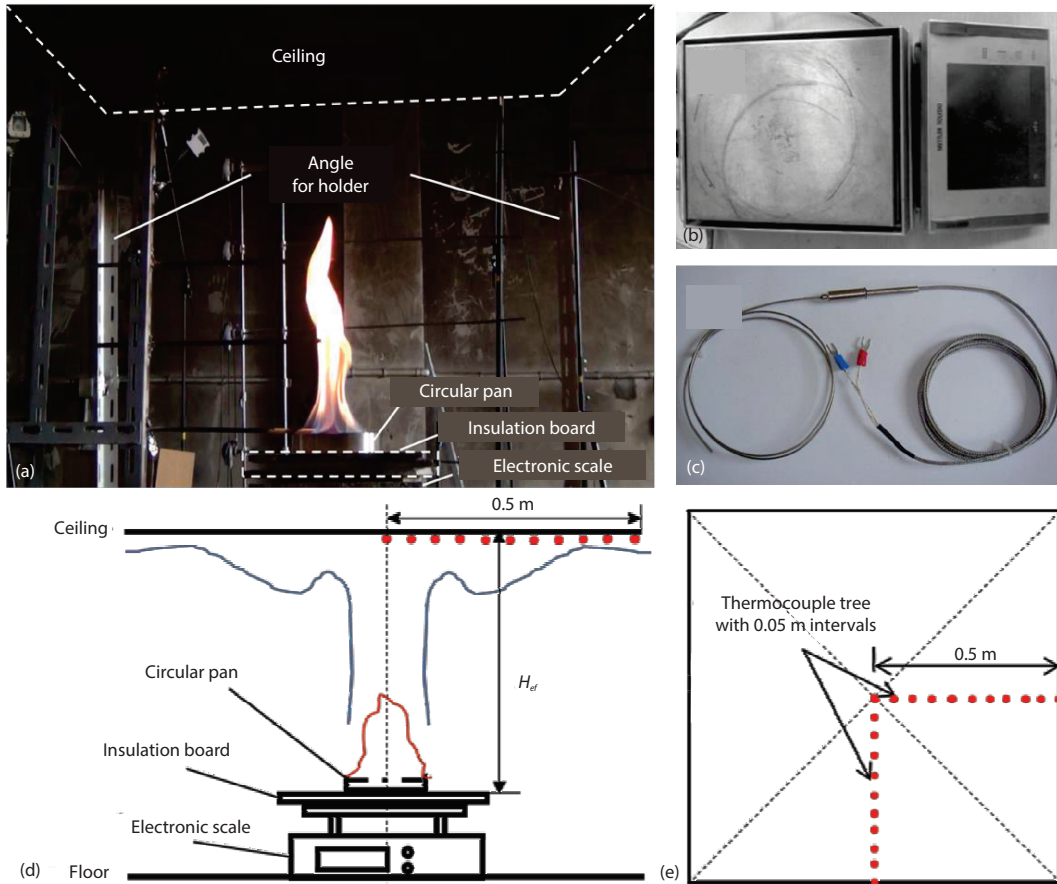


Figure 2. Photos and schematic diagram of the experiments; (a) typical photo during the test, (b) electronic scale, (c) armored K-type thermocouple, (d) schematic diagram of the test, and (e) arrangement of thermocouples beneath the ceiling

Table 1. Summary of experimental configurations

Fuel	Density [kgm ⁻³]	Exp. No.	H_{ef} [m]	Pan diameter [m]	Heat release rate [kW]	Flame height [m]
Ethanol	789	1	0.55	0.10	1.84	0.23
		2	0.55	0.14	3.64	0.30
		3	0.55	0.20	7.72	0.39
		4	0.95	0.10	1.84	0.23
		5	0.95	0.14	3.64	0.30
		6	0.95	0.20	7.72	0.39
<i>n</i> -heptane	679	7	0.95	0.10	3.20	0.32
		8	0.95	0.14	6.48	0.42
		9	0.95	0.20	13.95	0.55
Jet-A	792	10	0.95	0.10	2.53	0.28
		11	0.95	0.14	5.43	0.38
		12	0.95	0.20	12.29	0.52

The vertical distance between the ceiling and the bottom of the fuel pan was defined as the effective ceiling height, H_{ef} , to correlate the experimental results in following discussion. Measurements of the vertical temperature distribution below the ceiling show that the maxima occur at a distance about 1% of the ceiling height [12]. Two effective ceiling heights, 0.95 m and 0.55 m (only for ethanol fuel), were tested in current study to examine the effect of ceiling height. Thus, the thermocouples were mounted below the ceiling at a distance of 1 cm for all the tests to monitor the maximum temperatures. The armored K-type thermocouples, $\Phi = 0.5$ mm, with measurement range of 0~1100 °C were arranged along the two perpendicular directions, and the interval between adjacent ones was 0.05 m, as shown in fig. 2(e). To consider the radiation effect upon the thermocouples, Luo's method [20] was used to correct the error of the measured temperature and the uncertainty will be less than 10%. The experimental configurations are summarized in tab. 1. Each test was repeated at least three times to guarantee the repeatability. For all the experiments, the environmental temperature and relative humidity in the test room were 10 ± 3 °C and $20 \pm 5\%$, respectively.

Results and discussion

Experimental results

The fires in current study are assigned to be thin-layer pool fires, the burning process of which can be partitioned into four typical stages, *i. e.* (I) pre-steady stage, (II) quasi-steady stage, (III) boiling stage, and (IV) decay stage [15, 16, 18]. Considering the stable flame appearance and balanced heat feedback to the fuel surface, only the data in the quasi-steady burning stage are selected to be applied for analysis. The typical images during the quasi-steady burning stage for the three fuels are illustrated in fig. 3, where the differences between different fuel types and pool dimensions can be clearly observed. Generally, the flame height increases with the pool size for all the fuels. The ethanol fires exhibit blue flame bases and white and bright flame, which represents the lower soot production. In contrast, the moderately-sooting *n*-heptane fires show the yellow flames with relatively more soot yield, while the heavily-sooting jet-A fires show the deep yellow flames and even red light around the flames, which conforms with the statement in [16].

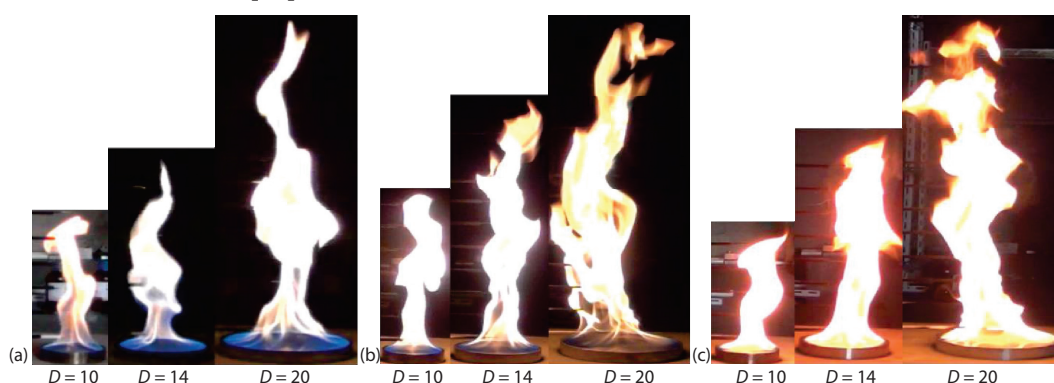


Figure 3. Typical images of the three fuels with different pool dimensions; (a) ethanol, (b) *n*-heptane, and (c) jet-A

Figure 4 presents the typical results of mass loss rate of *n*-heptane pool fire. The accurate delimitation of quasi-steady stage can be achieved by the derivative of mass loss rate using the criterion of $|d\dot{m}/dt \leq 0.02| \text{ g}\cdot\text{s}^{-2}$, as indicated in fig. 4. It must be noted that in different

experiments, the time intervals are similar but with slight difference. Correspondingly, the temperature data over the quasi-steady stage are averaged for the following discussion.

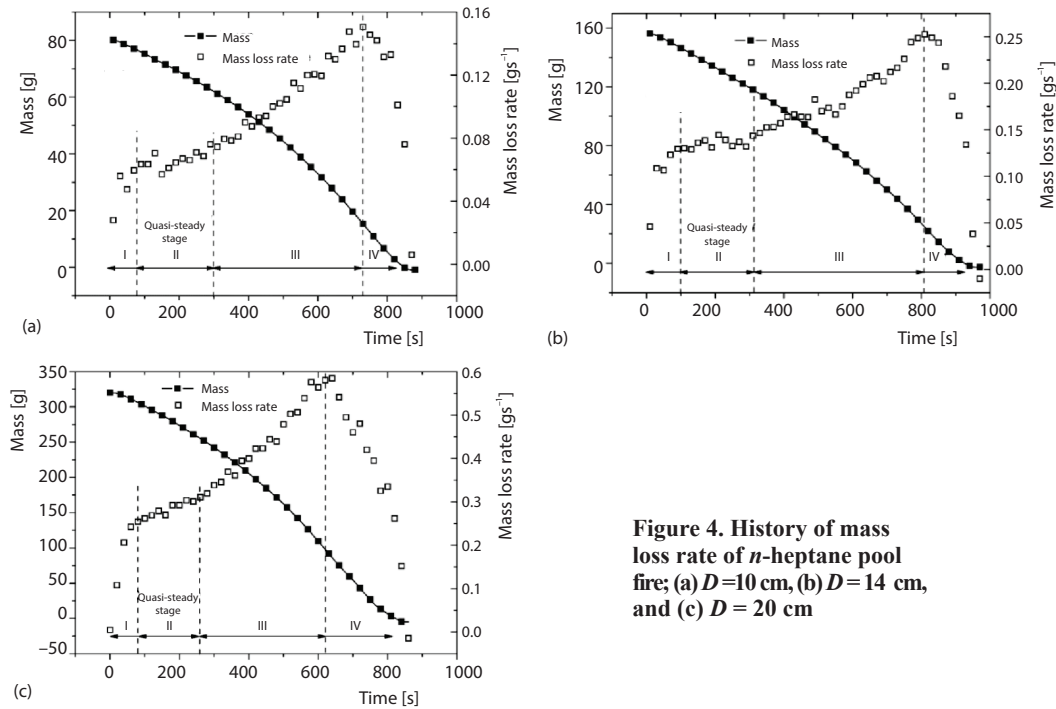


Figure 4. History of mass loss rate of *n*-heptane pool fire; (a) $D=10$ cm, (b) $D=14$ cm, and (c) $D=20$ cm

In current study, the research focus is the maximum excess temperature of the smoke flow induced by the weak plume driven ceiling jet, *i. e.* the flame height is smaller than the effective ceiling height. Zhou *et al.* [15] performed a unified analysis on the flame heights of pool fires at different altitude, and demonstrated that the dimensionless flame height z_f/D at high altitude also follows the conventional equation which covers the entire diffusion regime of Q^* ($0.12 < Q^* < 1.2 \cdot 10^4$):

$$\frac{z_f}{D} = 3.7(Q^*)^{2/5} - 1.02 \quad (1)$$

where Q^* is the dimensionless heat release rate:

$$Q^* = \frac{\dot{Q}}{\rho_\infty c_p T_\infty \sqrt{g} D^{5/2}} \quad (2)$$

where \dot{Q} is the heat release rate, ρ_∞ – the air density, c_p – the specific heat of air, T_∞ – the ambient temperature, g – the gravitational acceleration. For the quasi-steady burning stage, the heat release rate, \dot{Q} , can be calculated from the expression:

$$\dot{Q} = \dot{m} \Delta H_c \quad (3)$$

where \dot{m} is the mass loss rate, ΔH_c – the heat of combustion. Based on eqs. (1)-(3), the mean flame height during the quasi-steady burning stage can be obtained, and the results are listed in the last column of tab. 1. It is shown that the flame will not touch the ceiling for all the configurations.

Correlation on the maximum excess temperature

Based on the experiments with the heat release rates ranging from 668-98 MW and ceiling height from 4.6~15.5 m, Alpert developed easy-to-use correlations to quantify the maximum ceiling temperature rise as the dimensionless distance away from the plume axis (r/H_{ef}) is not larger than 0.18 [12]:

$$\Delta T_{\max}(H) = C_1 \frac{\dot{Q}^{2/3}}{H^{5/3}} \tag{4}$$

where C_1 is a constant which equals to 16.9 in Alpert's correlation. However, certain constraints should be understood when applying this correlation in the analysis of ceiling jet flow. The correlation was established from the test data to apply in cases where the fire source is at least a distance 1.8 times the ceiling height from the enclosure walls to guarantee no accumulated warm upper layer under the ceiling [1, 12]. In effect, the experimental results [6] in model-scale tunnel with the ratio of ceiling height to the distance from the wall equivalent to were also in accordance with the predicted results by eq. (4). In addition, theoretical analysis of maximum gas temperature beneath a tunnel ceiling based on a plume theory was performed by Li *et al.* [7], and their results also presented the similar proportional relationship with $C_1 = 17.5$ as the ventilation velocity is quite small. The cross-section of the model tunnel employed in their experiments is square, *i. e.* the ratio mentioned before equals to 0.5, which is narrow to result in the hot smoke accumulation and thereby higher gas temperature [7].

The experiments in current study are conducted under an unconfined ceiling, and the nearest wall is about 3.5 times the ceiling height. Thus, it can be regarded as an open space without any smoke accumulation, similar to Alpert's experimental conditions. The maximum excess temperatures of the twelve experimental configurations are plotted in fig. 5 together with Alpert's and Li's models. It clearly shows that the maximum temperatures at high altitude environment are higher than the results predicted by the models established under normal pressure. This may be attributed to the flame stretching and weaker air entrainment under low pressure environment [15, 21]. To well understand the pressure effect on the maximum ceiling temperature, the ideal plume model is taken into account to decipher the experimental results.

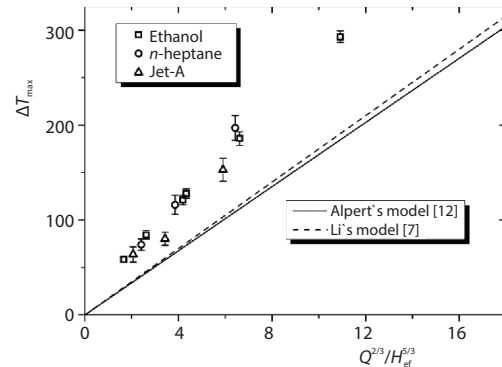


Figure 5. The maximum ceiling temperature vs. $Q^{2/3}/H_{ef}^{5/3}$

Considering the assumption of an ideal plume, the mass-flow rate of an axisymmetric fire plume at a height of z in the open can be originally expressed [22]:

$$\dot{m}_p(z) = \pi \rho_\infty \left(\frac{6}{5} \alpha z \right)^2 \left(\frac{25 \dot{Q}_c g}{48 \alpha^2 \pi c_p T_\infty \rho_\infty} \right)^{1/3} z^{-1/3} = 2.48 \left(\frac{g \rho_\infty^2 \alpha^4 \dot{Q}_c}{c_p T_\infty} \right)^{1/3} z^{5/3} \tag{5}$$

where α is the air entrainment coefficient, \dot{Q}_c – the convective heat of combustion. As the altitude increases, the ambient pressure will decrease, and the air density is proportional to ambient pressure, *i. e.* $\rho_\infty \sim P$. Through the comparison on the experimental results at plateau and plain, Tang *et al.* [21] also found that the air entrainment coefficient in Lhasa is only 0.8 time of that

in Hefei (a sea-level city). Thus, these two parameters need to be taken into consideration in correlating the current temperature data, and the eq. (5) can be approximated:

$$\dot{m}_p(z) \sim P^{2/3} \alpha^{4/3} \dot{Q}_c^{1/3} z^{5/3} \quad (6)$$

Convection is the dominant mode of heat transfer for the case of weak plumes impinging on ceilings. The convective heat of combustion is generally estimated:

$$\dot{Q}_c = (1 - X_r) \dot{Q} \quad (7)$$

where X_r is the radiative fraction of fuel, which has been experimentally testified to be weakly dependent on pressure due to the counteracting effects of the decrease in flame surface area and the increase in soot formation under lower pressure [15]. Thus, it is reasonable to assume a constant value for a given fuel. For ethanol with little soot generated, the total heat release rate is roughly the same as the convective heat release rate, *i. e.* $X_r \approx 0$ [1]. Besides, $X_r = 0.3$ for moderately-sooting *n*-heptane fuel, and $X_r = 0.4$ for heavily-sooting jet-A fuel [4, 22]. By introducing the radiative fractions, different fuel types are now taken into consideration in the correlation.

Furthermore, in the ideal plume or the point-source plume, the virtual source term is used to compensate to the difference between the actual fire source and the ideal point source [23]. The height of the virtual origin z_0 can be calculated:

$$z_0 = -1.02D + 0.083\dot{Q}^{2/5} \quad (8)$$

Because the pan dimensions used in current study are relatively large compare with the dimension of the ceiling, the virtual origin is reasonably introduced to modify the form of the ideal plume. Thus, the eq. (6) can be further transformed:

$$\dot{m}_p(z) \sim (1 - X_r)^{1/3} P^{2/3} \alpha^{4/3} \dot{Q}^{1/3} (z - z_0)^{5/3} \quad (9)$$

The average excess temperature of the fire plume at the effective ceiling height can be expressed:

$$\Delta T(H_{ef}) = \frac{\dot{Q}_c}{m_p(H_{ef})c_p} = \xi(P, \alpha) \frac{\dot{Q}^{2/3}}{(H_{ef} - z_0)^{5/3}} (1 - X_r)^{2/3} \quad (10)$$

Previous researchers have indicated that the maximum smoke temperature rise of the plume is proportional to the eq. (10), and the proportionality coefficient can be determined experimentally [6, 7]:

$$\Delta T_{\max} \sim \Delta T(H_{ef}) \quad (11)$$

Combining eqs. (9)-(11), the maximum smoke temperature at the measuring points can be expressed:

$$\Delta T_{\max} \sim \alpha^{-4/3} \frac{\left(\frac{\dot{Q}}{P}\right)^{2/3}}{(H_{ef} - z_0)^{5/3}} (1 - X_r)^{2/3} \quad (12)$$

The maximum temperatures beneath the ceiling in current study are plotted in fig. 6 according to eq. (12). For comparison, the experimental results under normal pressure obtained by Ji *et al.* [6], which have been verified to be perfectly fitted with Alpert's model, are also presented. The fire sources used in their tests are not circular, and thus the equivalent radiuses are employed based on the equivalent area of the fire source. The result shows that the data under normal and subatmospheric pressures concentrate with each other by employing the eq. (12),

and the fitted result gives the following expression with the adjusted coefficient of determination $R^2 = 0.966$.

$$\Delta T_{\max} = 25.5\alpha^{-4/3} \frac{\left(\frac{\dot{Q}}{P}\right)^{2/3}}{(H_{ef} - z_o)^{5/3}} (1 - X_r)^{2/3} \quad (13)$$

Conclusion

The maximum excess temperature beneath an unconfined horizontal ceiling at high-altitude environment was experimentally examined by means of pool fires with different dimensions and fuel types. Experimental findings revealed that Alpert's model for predicting the maximum smoke temperature under the ceiling was not applied at high-altitude environment, and the current measured temperatures were clearly higher than the predicted values. A new model based on the ideal plume was established to correlate the experimental data by taking the pressure, entrainment coefficient, virtual point source and fuel type into considerations, see eq. (13). The results showed that proposed model could well unify the data under normal pressure and high-altitude environment. Given the significant difference in temperature, fire engineers must be aware of the effect of altitude in current building designs, as the temperature beneath the ceiling increases when the fire occurs at high altitude. Developed correlation can be applied in the fire safety design of buildings at high altitude, while it should not be applied in the narrow spaces (such as corridors, tunnels and, etc.) unless further validation is conducted.

Acknowledgment

This research was financially supported by the National Natural Science Foundation of China (No. 51376172, 51408181 and 50909058), Natural Science Foundation of Shanghai (No. 16ZR1414600) and the grant from the Research Grants Council of the Hong Kong Special Administrative Region (Project No. CityU 11301015). The authors deeply appreciate that.

Nomenclature

c_p – specific heat of air, [$\text{Jkg}^{-1}\text{K}^{-1}$]
 C_1 – constant, [–]
 D – diameter of the oil pan, [m]
 g – gravitational acceleration, [ms^{-2}]
 H_{ef} – effective ceiling height, [m]
 ΔH_c – heat of combustion, [kJkg^{-1}]
 \dot{m} – mass loss rate, [gs^{-1}]
 \dot{m}_p – mass-flow rate of fire plume, [gs^{-1}]
 P – ambient pressure, [kPa]
 \dot{Q} – heat release rate, [kW]
 \dot{Q}^* – dimensionless heat release rate, [–]
 \dot{Q}_c – convective heat release rate, [kW]

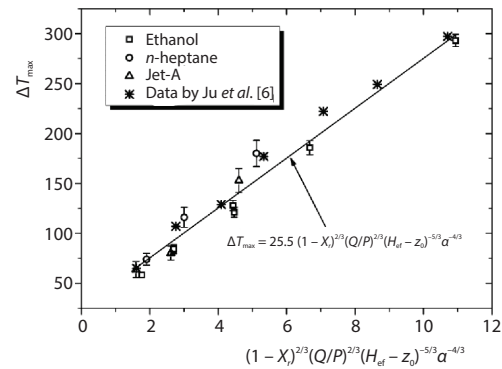


Figure 6. A proposed correlation of maximum ceiling smoke temperature for different ambient pressure

r – distance away from the plume axis, [m]
 T_o – ambient temperature, [K]
 ΔT_{\max} – the maximum excess temperature, [K]
 X_r – radiation fraction, [–]
 z – vertical height above the pool surface, [m]
 z_f – flame height, [m]
 z_o – height of the virtual origin, [m]

Greek symbols

α – entrainment coefficient, [–]
 ρ_o – ambient pressure, [kgm^{-3}]

References

- [1] Dinunno, P. J., *SFPE Handbook of Fire Protection Engineering* (ed. 3rd), National Fire Protection Engineering, Quincy, Mass., USA, 2002

- [2] He, Y. P. et al., Smoke Venting and Fire Safety in an Industrial Warehouse, *Fire Safety Journal*, 37 (2002), 2, pp. 191-215
- [3] Bystrom, A., et al., Full-Scale Experimental and Numerical Studies on Compartment Fire under Low Ambient Temperature, *Building and Environment*, 51 (2012), May, pp. 255-262
- [4] Gutierrez-Montes, C., et al., Experimental Data and Numerical Modelling of 1.3 and 2.3 MW Fires in a 20 m³ atrium, *Building and Environment*, 44 (2009), 9, pp. 1827-1839
- [5] Gutierrez-Montes, C., et al., Numerical Model and Validation Experiments of Atrium Enclosure Fire in a New Fire Test Facility, *Building and Environment*, 43 (2008), 11, pp. 1912-1928
- [6] Ji, J., et al., A Simplified Calculation Method on Maximum Smoke Temperature under the Ceiling in Subway Station Fires, *Tunnelling and Underground Space Technology*, 26 (2011), 3, pp. 490-496
- [7] Li, Y. Z., et al., The Maximum Temperature of Buoyancy-Driven Smoke Flow Beneath the Ceiling in Tunnel Fires, *Fire Safety Journal*, 46 (2011), 4, pp. 204-210
- [8] Hu, L. H., et al., On the Maximum Smoke Temperature under the Ceiling in Tunnel Fires, *Tunnelling and Underground Space Technology*, 21 (2006), 6, pp. 650-655
- [9] Wang, J., et al., Early Stage of Elevated Fires in an Aircraft Cargo Compartment: A Full Scale Experimental Investigation, *Fire Technology*, 51 (2015), 5, pp. 1129-1147
- [10] Wang, J., et al., Experiment Investigation on the Influence of Low Pressure on Ceiling Temperature Profile in Aircraft Cargo Compartment Fires, *Applied Thermal Engineering*, 89 (2015), Oct., pp. 526-533
- [11] Chen, S. J., et al., Fire Detection Using Smoke and Gas Sensors, *Fire Safety Journal*, 42 (2007), 8, pp. 507-515
- [12] Alpert, R. L., Calculation of Response Time of Ceiling-Mounted Fire Detectors, *Fire Technology*, 8 (1972), 3, pp. 181-195
- [13] Alpert, R. L., Turbulent Ceiling-Jet Induced by Large-Scale Fires, *Combustion Science and Technology*, 11 (1975), 5-6, pp. 197-213
- [14] Heskestad, G., et al., The Initial Convective Flow in Fire, *Symposium (International) on Combustion*, 17 (1979), 1, pp. 1113-1123
- [15] Zhou, Z. H., et al., Experimental Analysis of Low Air Pressure Influences on Fire Plumes, *International Journal of Heat and Mass Transfer*, 70 (2014), Mar., pp. 578-585
- [16] Liu, J. H., et al., Experimental Study on Burning Behaviors of Liquid Fuels with Different Sooting Levels at High Altitude, *Thermal Science*, 21 (2016), 6A, pp. 2533-2541
- [17] Wang, Y., et al., Fire Detection Model in Tibet Based on Grey-Fuzzy Neural Network Algorithm, *Expert Systems with Applications*, 38 (2011), 8, pp. 9580-9586
- [18] Liu, J. H., et al., Investigation of Enclosure Effect of Pressure Chamber on the Burning Behavior of a Hydrocarbon Fuel, *Applied Thermal Engineering*, 101 (2016), May, pp. 202-216
- [19] Hamins, A., et al., Heat Feedback to the Fuel Surface in Pool Fires, *Combustion Science and Technology*, 97 (1994), 1-3, pp. 37-62
- [20] Luo, M. C., et al., Application of Field Model and Two-Zone Model to Flashover Fires in a Full-Scale Multi-Room Single Level Building, *Fire Safety Journal*, 29 (1997), 1, pp. 1-25
- [21] Tang, F., et al., An Experimental Investigation on Temperature Profile of Buoyant Spill Plume from Under-Ventilated Compartment Fires in a Reduced Pressure Atmosphere at High Altitude, *International Journal of Heat and Mass Transfer*, 55 (2012), 21, pp. 5642-5649
- [22] Karlsson, B., et al., *Enclosure Fire Dynamics*, Boca Raton, CRC Press, Fla., USA, 1999
- [23] Heskestad, G., Virtual origins of fire plumes, *Fire Safety Journal*, 5 (1983), 2, pp. 109-114